Hindawi
Science and Technology of Nuclear Installations
Volume 2022, Article ID 2354978, 8 pages
https://doi.org/10.1155/2022/2354978

Research Article

Investigation of the Flow and Heat Transfer Characteristics and Erosion Law of Particulate in LBE on the Subchannel

Bingheng Zhu, Qi Xu, and Pengxiang Li

School of Electric Power, North China University of Water Resources and Electric Power, Zhengzhou 450040, China

Correspondence should be addressed to Qi Xu; hnxuq@ncwu.edu.cn

Received 16 December 2021; Revised 18 January 2022; Accepted 23 February 2022; Published 22 March 2022

Academic Editor: Leon Cizelj

A triangle subchannel model was established to study the flow and heat transfer characteristics of lead-bismuth eutectic (LBE) alloy and the erosion rate of the core channel by the particulate in LBE. Under different inlet velocities, particle types, particle diameters, and particle concentrations, the erosion law of the channel wall in LEB was investigated by using a discrete phase model (DPM). The results of this study showed that with the increase of inlet velocity, the outlet temperature of the LEB decreases and the heat transfer capacity was strengthened. The increase of inlet velocity will lead to the increase of erosion rate on the wall, and the change is exponential. The erosion rate of particulate in the low concentration is small but cannot be ignored; with increasing concentration of particulates, the erosion of the wall by particulates becomes serious. The effect of particulate density on the wall erosion rate can be ignored. The effect of changing the particle size on the erosion rate is more significant when the particle size is small, and at the same time, the erosion rate of the particles on the wall increases with the increase of the particle size.

1. Introduction

Liquid lead-bismuth eutectic alloy [1–3] was considered to be used for available as a coolant in the Generation IV lead-cooled fast reactor (LFR) due to its good neutronic properties, low melting point, and other characteristics. Many scholars at home and abroad have conducted experimental and numerical studies on the heat transfer performance of LBE. Wang et al. [4] conducted an experimental study on the heat transfer efficiency of LBE with helium exchange and found that the overall heat transfer coefficient of the exchanger increased with inlet temperature. Zhang et al. [5] studied the heat transfer characteristic of LBE in the round pipeline and fitted a heat transfer relationship between the Nu and the Pe of the LBE in the circular tube. Cheng and Tak [6] carried out CFD studies on flow and heat transfer characteristics of LBE in triangular subchannels and square subchannels and found that the turbulence distribution in triangular and square channels was similar.

With scholars' research on LBE, it has been found that LBE itself is corrosive. The LBE in the pipeline will scour and corrode the oxide film on the surface of the pipeline [7–9] and produce solid scum [6], and these particulate matters locally aggregate, and the deposition effect will increase the thermal resistance of the wall and affect the safe operation of the reactor. Aiming at the research on the movement and deposition of particulate matter in LBE, Du et al. [10] studied the erosion of the pipeline by the particulate matter contained in lead and bismuth in the bent pipe and found that the angle of the bend has a meaningful impact on the erosion of particulate matter. Liu et al. [11] designed a cylindrical pipe for depositing particulate matter and studied the antideposition ability of the pipe against particulate matter under different temperature differences and particle diameters. Chen et al. [12] studied the thermophoretic velocity of different particles in R134a, engine oil, ethyl glycol, water, and LBE and found that stainless steel particles had the lowest thermophoretic velocity in LBE.

In previous studies, the exploration of the movement and deposition of particulate matter in LBE has mainly focused on round straight pipes or curved pipes, while little has been reported on the erosion of the core channels in nuclear power plants by particulate matter in lead-bismuth. Therefore, this paper first establishes the model of the

subchannel and introduces the geometric configuration and boundary conditions adopted in the study in detail. Then, the mesh independence and model validation are performed to ensure the accuracy of the calculation results. Finally, the flow and heat transfer characteristics of LBE in the subchannel and the erosion law of particulates on the wall under the influence of different parameters are obtained. The research results can provide theoretical support for the design of LFR.

2. Research Object

2.1. Geometric Model. The geometric model studied in this paper is shown in Figure 1. The computational area is the triangular area within the subchannel, and the model was built by NX10.0. The fuel rod bundle spacing $P = 11.2$ mm, the fuel rod diameter $D = 8$ mm, and the grid distance ratio $P/D = 1.4$. The fuel rod length $Z = 1000$ mm.

2.2. Mesh Division. The mesh of the channel is hexahedrally meshed by ICEM, and the boundary layer encryption is used on the bar beam surface in order to accurately capture the turbulence and heat transfer characteristics in the near-wall region. The mesh division is shown in Figure 2.

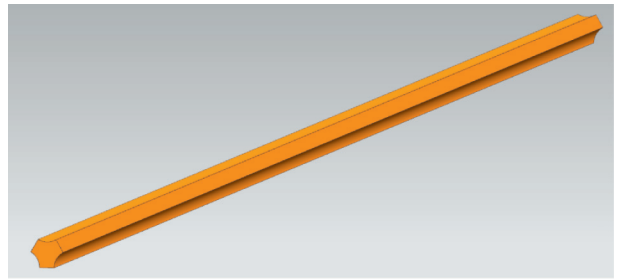

Figure 1: Geometric model.

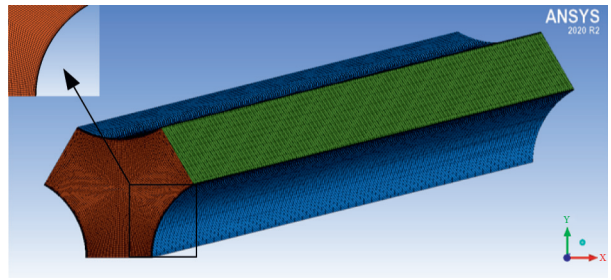

Figure 2: Mesh of the fluid domain.

3. Research Methodology

3.1. The RNG k-ε Turbulence Model. RNG k-ε turbulence model was used for fluid flow calculation in a continuous phase. Since LBE belongs to low Prandtl number fluid, in order to increase the accuracy of calculation, it is necessary to modify the turbulent Prandtl number when calculating LBE in FLUENT, and it is necessary to re-establish the Pr_t model suitable for LBE. After the comparative study of heat transfer results of LBE under different turbulent Prandtl number models by Wang [13], it is found that the result of the Cheng and Tak [14] model has a good match with the experimental results, so the UDF was used to insert this Pr_t model into FLUENT for the calculation of LBE.

$$\mathrm{Pr}_t \begin{cases} 4.12, & \mathrm{Pe} \le 1000, \\ \dfrac{0.01Pe}{\left[0.018\mathrm{Pe}^{0.8} - (7.0 - A)\right]^{1.25}}, & 1000 < \mathrm{Pe} \le 6000, \end{cases} \tag{1}$$

$$A = \begin{cases} 5.4 - 9 \times 10^{-4} Pe, & 1000 < \mathrm{Pe} \le 2000, \\ 3.6, & 2000 < \mathrm{Pe} \le 6000. \end{cases}$$

3.2. The Discrete Phase Model (DPM). The particle phase uses the DPM to simulate the movement of the particles in the channel. The DPM force model can be derived as follows:

$$\frac{\mathrm{d}u_p}{\mathrm{d}t} = F_D\left(\vec{u} - \vec{u}_p\right) + \frac{\vec{g}\left(\rho_p - \rho\right)}{\rho_p} + \vec{F}_x, \tag{2}$$

where u is the LBE velocity, m/s; u_p is the particle phase velocity, m/s; ρ and ρ_p are the density of fluid and particles, respectively, kg/m^3; F_x is the additional force in the x-direction, N; F_D is the trapping force, N, which is calculated by

$$F_D = \frac{18\mu}{\rho_p d_p^2} \frac{C_D \mathrm{Re}}{24}, \tag{3}$$

where μ is the LBE viscosity, Pa•s; dp is the particle diameter, m; C_D is the coefficient of traction, which is calculated by

$$C_D = \frac{24}{\mathrm{Re}}\left(1 + b_1 \mathrm{Re}^{b_2}\right) + \frac{b_3 \mathrm{Re}}{b_4 + \mathrm{Re}},$$

$$b_1 = \exp\left(2.3288 - 6.4581\varphi + 2.4486\varphi^2\right),$$

$$b_2 = 0.0964 + 0.5565\varphi,$$

$$b_3 = \exp\left(4.905 - 13.8944\varphi + 18.4222\varphi^2 - 10.2599\varphi^3\right),$$

$$b_4 = \exp\left(1.4681 + 12.2584\varphi - 20.7322\varphi^2 + 15.8855\varphi^3\right), \tag{4}$$

where φ is the shape factor.

The model for calculating the erosion rate can be defined by

$$R_{\mathrm{erosion}} = \sum_{p=1}^{P} \frac{m_p Q\left(d_p\right) f(\theta) u_p^{b(v)}}{A_{\mathrm{face}}}, \tag{5}$$

where p is the number of particulate collisions, $p = 1, \ldots, P$; m_p is the mass flow rate of the particles; $Q(d_p)$ is the function of particle diameter, taking the value of 1.8×10^{-9}; θ is the collision angle of the particle to the wall; $f(\theta)$ is the function of intrusion angle; $b(v)$ is the relative rate function, taking the value of 2.6; and A_{face} is the area of the wall calculation cell. When calculating the erosion of the core wall by the

particles carried by the LBE in FLUENT, the intrusion angle function is set with reference to the work of Edwards [15, 16], Finnie [17], Mclaury [18]. The specific setting values are shown in Table 1.

The normal recovery coefficient [19] and tangential recovery coefficient [20, 21] are defined in Fluent.

$$e_N = 0.993 - 0.0307\theta + 4.75 \times 10^{-4}\theta^2 - 2.61 \times 10^{-6}\theta^3, \quad (6)$$

$$e_T = 0.998 - 0.029\theta + 6.43 \times 10^{-4}\theta^2 - 3.56 \times 10^{-6}\theta^3. \quad (7)$$

3.3. Boundary Condition Setting. The finite volume method is utilized to calculate the erosion of particulate matter in LBE on the subchannel, and the physical properties of LBE [22] can be found in Table 2. The LBE flows in the channel from bottom to top, and the inlet and outlet are configured as velocity inlet and pressure outlet, respectively. The outer wall surface is set as shown in Figure 3, the cladding surface is set to uniform heat flux, the other three surfaces are set as symmetry, the turbulence model is RNG k-ε turbulence model, and the COUPLE algorithm is used to solve the coupled pressure-velocity. Finally, the calculation is considered converged when the residuals of all monitored variables are less than 10^{-6}.

3.4. Grid-Independent Solutions. The grid quality has a great influence on the numerical calculation results, and the grid-independent solution is carried out by using three grid division schemes with different boundary layer encryption methods to obtain the grid numbers of 3.3×10^5, 4.4×10^5, and 8×10^6. The wall temperature distribution of different mesh cases is shown in Figure 4. Continuing to increase the number of grids, there is no significant change in the calculation results from 4.4×10^5 to 8×10^6, so the grid number of 4.4×10^5 was used for the numerical calculation of this paper.

Figure 5 shows the calculated results of the developed model are compared with Mikityuk [23] heat transfer correlation (see equation (8)) and Ushakov [24] heat transfer correlation (see equation (9)). As can be seen from Figure 5, the calculated results in this paper are slightly lower than the predicted value of the equations, but the error is within 10%, so the accuracy of the calculated model in this paper can be proved.

$$\mathrm{Nu} = 0.047\left(1 - e^{-3.8(X-1)}\right)\left(\mathrm{Pe}^{0.77} + 250\right), \quad 30 \le \mathrm{Pe} \le 5000,\ 1.1 \le X \le 1.95, \quad (8)$$

$$\mathrm{Nu} = 7.55X - \frac{20}{X^{13}} + \frac{0.041}{X^2}\mathrm{Pe}^{0.56+0.19X}, \quad 1 \le \mathrm{Pe} \le 4000,\ 1.3 \le X \le 2.0, \quad (9)$$

where Pe is Peclet numbers, and X is the pitch-to-diameter ratio for a tube bundle.

4. Results and Discussion

4.1. Velocity Analysis. With the established subchannel model, the velocity field in the core channel with an inlet temperature of 573 K, wall heat flow density of 30 kW/m^2, and inlet velocity of 0.3 m/s~1 m/s were analyzed, and the velocity distribution at different inlet velocities is shown in Figure 6.

Table 1: The intrusion angle function.

θ	$f(\theta)$
0	0
20	0.55
30	0.4
45	0.25
90	0.2
0	0

As depicted in Figure 6, the overall velocity of the LBE in the subchannel increases as the fluid inlet velocity increases. Due to the inlet effect, a slow region of increase in fluid velocity occurs in the front section of the subchannel, followed by the fully developed section, where the fluid velocity within the fully developed section is almost unchanged.

The velocity distribution of LBE in the fully developed section of the subchannel is shown in Figure 7 for an inlet velocity of 0.5 m/s which can be seen that the velocity distribution of the fully developed section of LBE in the subchannel has a Y-shaped distribution. The velocity is highest at the center of the core fluid domain and lowest at the walls. The reason for this distribution is the boundary layer effect and the compression of the fluid by the channel structure, where the fluid velocity is lower than the velocity at the center of the channel due to the boundary layer effect at the walls. At the same time, the three straight edges are set as symmetry, where the fluid can flow freely. Therefore, under the combined effect of wall extrusion and boundary layer effect, the velocity distribution is Y-shaped distribution.

4.2. Turbulent Energy Analysis. Taking the inlet velocity 0.5 m/s as an example for the turbulent energy distribution at the center of the subchannel, the calculation results are shown in Figure 8. It can be seen that similar to the velocity distribution, a valley is formed in the center of the core channel, which is a result of the smaller turbulent velocity rise and fall of the LBE at the center, while a peak is formed in the near-wall area on the outer surface of the fuel rod, which is caused by the peak of the radial velocity of the flow field in this area and the larger turbulent velocity rise and fall resulting in enhanced turbulence.

4.3. Temperature Analysis. With the established subchannel model, the temperature field in the core channel with an inlet temperature of 573 K, wall heat flow density of 30 kW/m^2, and inlet velocity of 0.3 m/s~1 m/s were analyzed, and the temperature distribution at different velocities is shown in Figure 9.

As shown in Figure 9, the temperature of LBE decreases with the increase of inlet velocity. It is because the increase of velocity, which reduces the time of fluid in the channel and makes the LBE unable to fully exchange heat.

Table 2: The physical parameters of LBE.

Name	Unit	Calculation equation
Density/ ρ	kg/m^3	$\rho = 11096 - 1.326T$
Specific heat/c_p	J/(kg·°C)	$c_p = 159 - 2.72 \times 10^{-2}T + 7.21 \times 10^{-6}T^2$
Thermal conductivity/ λ	W/(m·K)	$\lambda = 3.61 + 1.517 \times 10^{-2}T - 1.741 \times 10^{-6}T^2$
Viscosity/ η	Pa·s	$\eta = 4.94 \times 10^{-4} \exp(754.1/T)$

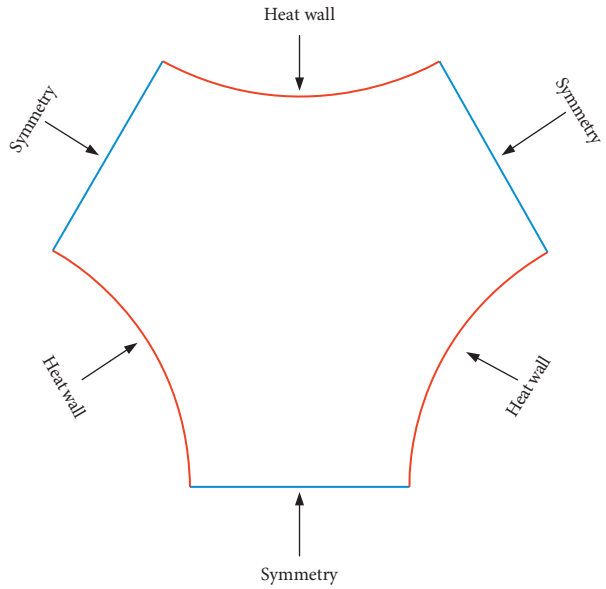

Figure 3: Boundary condition of the wall.

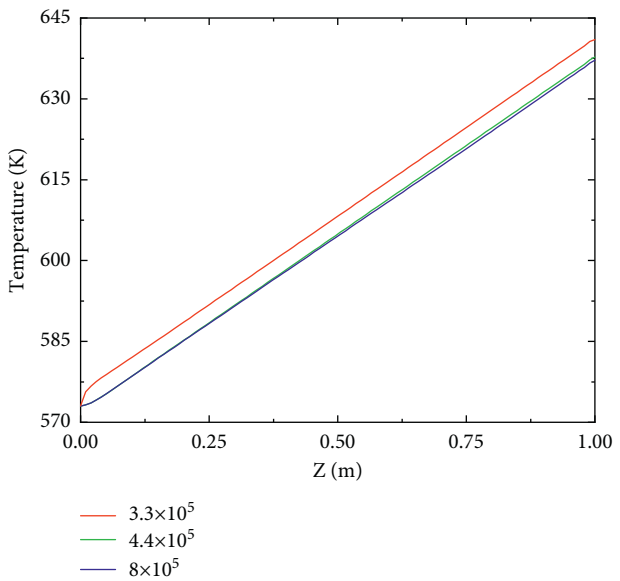

Figure 4: Temperature variation along the axial direction in mesh cases.

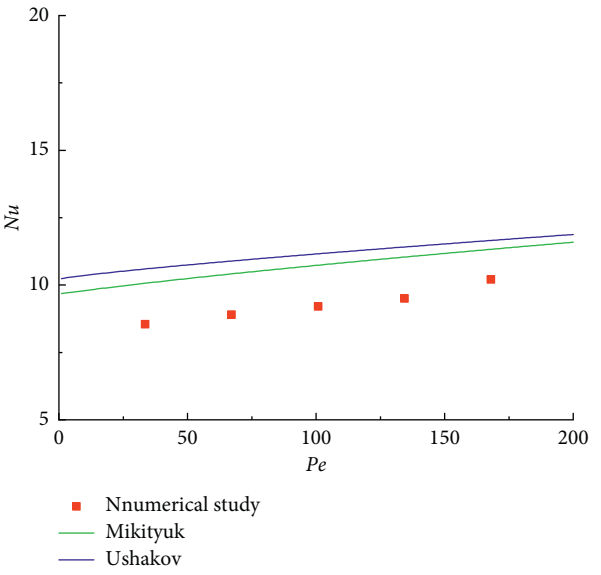

Figure 5: Comparison of numerical calculation results with experimental equations.

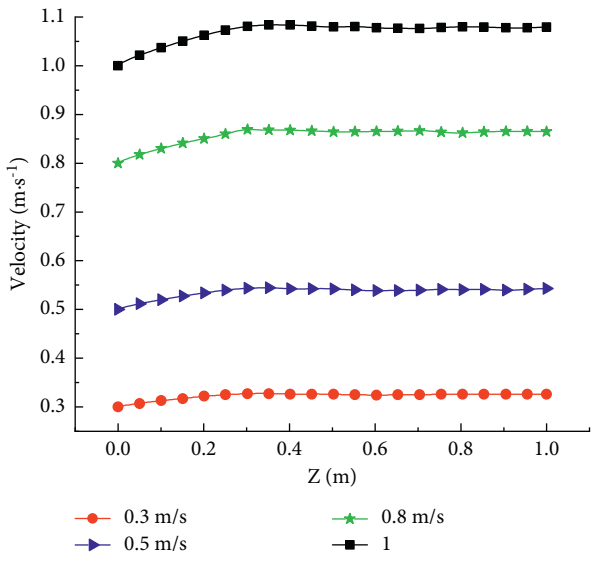

Figure 6: Velocity variation along the axial direction at different velocities.

Simultaneously, to quantitatively study the difference of heat transfer strength of liquid lead-bismuth in the core channel at different inlet velocities, the heat transfer coefficients h at the fully developed section $z = 500$ mm were calculated at velocities of 0.3, 0.5, 0.8, and 1 m/s, and the results were 40,269, 45,347, 53,236, and 57970 W/(m^2·k), respectively. The increase of velocity enhances the wall heat transfer coefficient, which is because the increase of velocity can increase the turbulence intensity, destroy the velocity boundary layer, strengthen the heat transfer capacity between fluid and wall, and increase the heat transfer coefficient.

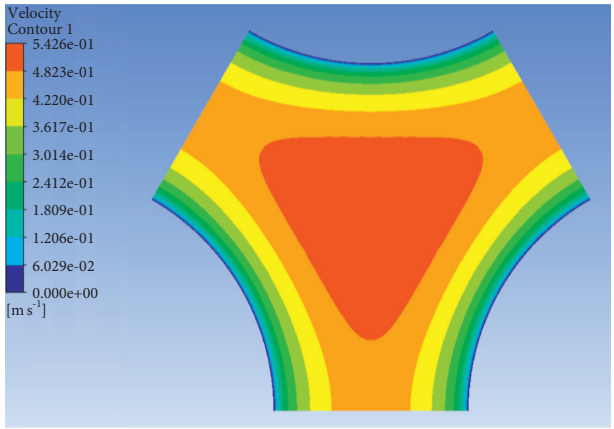

Figure 7: Velocity distribution.

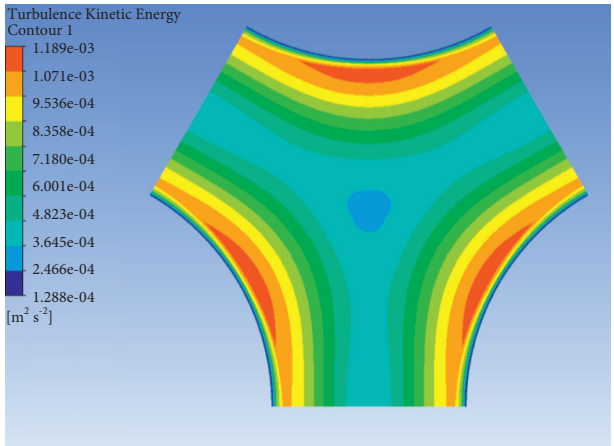

Figure 8: Turbulence kinetic energy distribution.

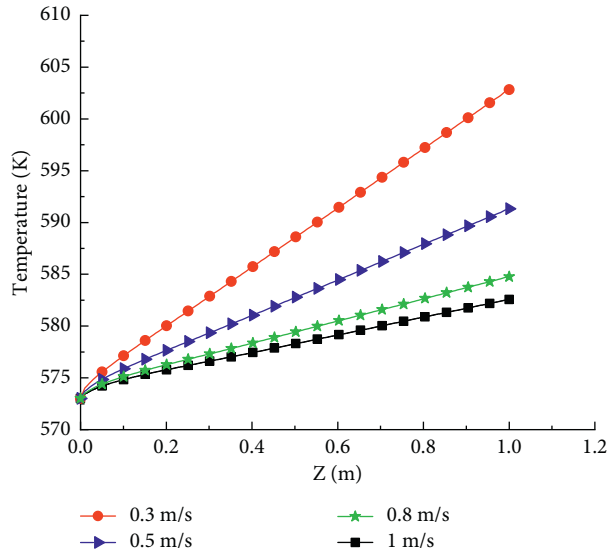

Figure 9: Temperature variation along the axial direction at different velocities.

Taking the inlet velocity of 0.5 m/s as an example, the temperature distribution at the center of the core channel is shown in Figure 10 It can be seen that in the fully developed

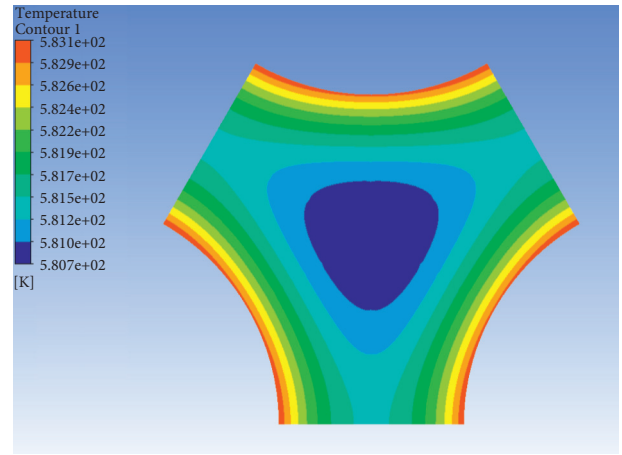

Figure 10: Temperature distribution.

section of the core channel fluid domain, the temperature has a Y-shaped distribution. The wall temperature is the highest, and the center temperature is the lowest. Compared to the temperature distribution of LBE in the circular channel [1], the triangular-like subchannel structure has a squeezing effect on the flow field distribution, which in turn causes the temperature distribution in the core fluid domain to be distorted. The field temperature distribution has a squeezing effect, which in turn causes the temperature distribution in the core fluid domain to be distorted.

4.4. Particle Concentration Distribution in the Subchannel. Through the established subchannel model, the particle concentration in the subchannel with the inlet temperature 573 K, wall heat flow density 30 kW/m^2, and inlet velocity 0.5 m/s is analyzed. The near-wall position of the channel was selected as the particle concentration distribution at the wall 0.1 mm. The particle mass concentration of the near-wall position and the center position is shown in Figure 11.

As shown in Figure 11, the inlet section of the channel wall concentration is higher than the concentration at the center of the channel, which is due to the inlet effect, the fluid in the channel when it first entered near the wall near the fluid velocity drops steeply to form stagnation, the deposition of particles in the vicinity of the inlet increases, and the particle density increases. As the process advances, the fluid velocity in the channel increases, the particles are less likely to be deposited, and the concentration of particles on the wall gradually decreases. It can also be seen from Figure 10 that the concentration of particles at the wall of the pipe shows an inverse pattern to the concentration at the center of the channel, which is due to the periodic migration and diffusion of particles between the center and near the wall during the whole flow process by the Brownian effect and turbulence.

4.5. Effect of Concentration and Type of Particle Matter on Erosion Rate. Figure 12 shows the comparative study of the erosion rate of different concentrations of particle matter on the core wall, and the particle size = 1 μm, inlet temperature 573 K, and mass flow velocity 0.029 kg/s are selected for the

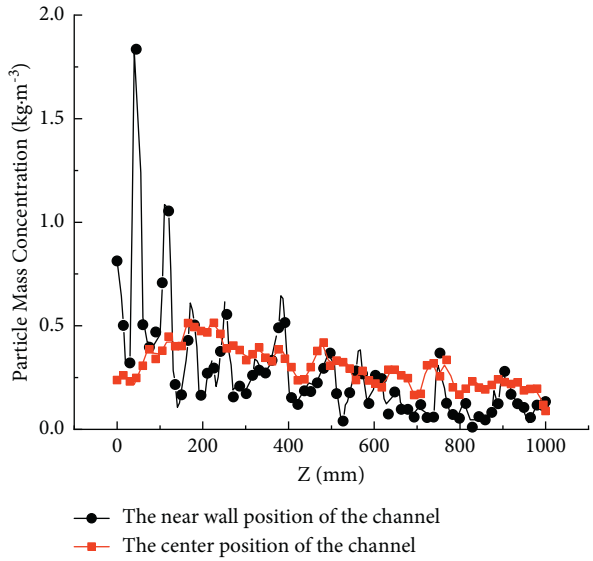

Figure 11: Particle concentration distribution along the axial direction at different positions.

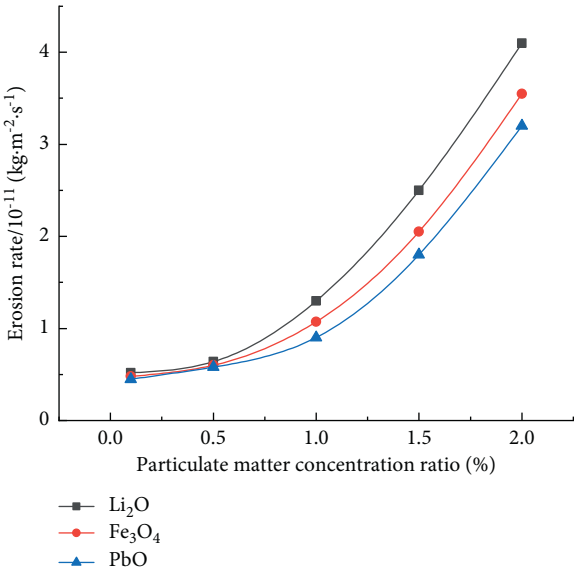

Figure 12: Effect of different concentrations and types on erosion rates.

calculation. Three kinds of particles, Li_2O, Fe_3O_4, and PbO, were selected for the study of five working conditions of 0.1%, 0.5%, 1%, 1.5%, and 2% of the fluid flow rate set for the particle concentration. It can be found from Figure 12 that the erosion rate of particulate matter on the wall increases with the increase of particle concentration, which is due to the fact that as the concentration of particulate matter increases, the number of particles in the channel increases, which increases the collision rate between them and the wall and therefore increases the erosion rate on the wall. At the same time, it can be seen that when the concentration of particulate matter is less than 1%, the change of particulate matter concentration has less effect on the wall erosion rate. When the concentration of particulate matter is greater than

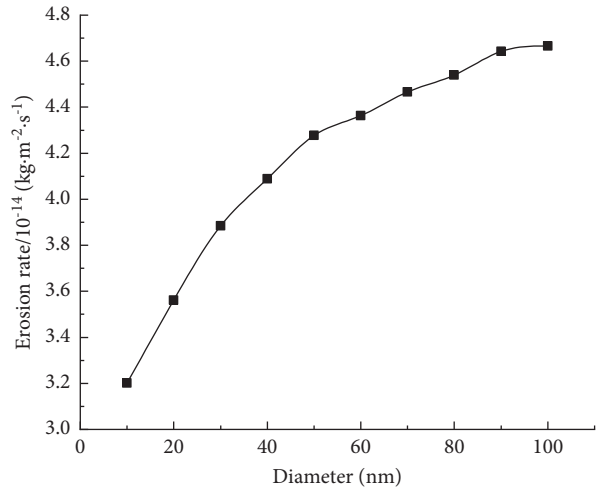

Figure 13: Effect of different diameters on erosion rates.

1%, the increase of the concentration of particulate matter leads to a sharp increase in the erosion rate.

It can also be seen from Figure 12 that the erosion rates of different types of particles on the wall are Li_2O, Fe_3O_4, and PbO in descending order. The reason for this phenomenon is because of the influence of the density of the three types of particles, where the order of density size is Li_2O(2013 kg/m^3) < Fe_3O_4(5180 kg/m^3) < PbO (9530 kg/m^3). As the density of the particles increases, the effect of the flow field changes on the movement of the particles becomes smaller, thus leading to a decrease in the impact velocity of the particles, so the erosion of the particles on the tube wall is reduced.

4.6. Effect of Particle Diameter on Erosion Rate. Figure 13 shows the calculated results of the effect of different particle diameters from 10 nm to 100 nm on the erosion rate of the triangle subchannel when the inlet mass flow velocity of LBE is 0.145 kg/s, the inlet temperature is 573 K, and the wall heat flow density is 30 kW/m^2.

Figure 13 illustrates that with the increase of particle size, the wall erosion rate gradually rises, and this is because as the particle diameter increases, the particles are more influenced by turbulence, which strengthens the wall erosion efficiency. When the particle diameter is greater than 60 nm, the effect of increasing particle diameter on the erosion rate gradually becomes slower, because the channel is placed vertically, the influence of gravity after the particle diameter becomes larger to offset part of the impact of fluid on the particles, reducing the impact of fluid turbulence, making the erosion rate increases slowly.

4.7. Effect of Inlet Velocity on Erosion Rate. Figure 14 shows the calculated results of the effect of the fluid inlet mass flow velocity of 0.029 kg/s~0.29 kg/s working condition particles on the erosion rate of the triangle subchannel at the LBE inlet temperature of 573 K and wall heat flow density of 30 kW/m^2.

It can be seen from Figure 14 that with the inlet velocity increases, the erosion rate of particles on the wall increases, and this is because the overall flow velocity in the channel

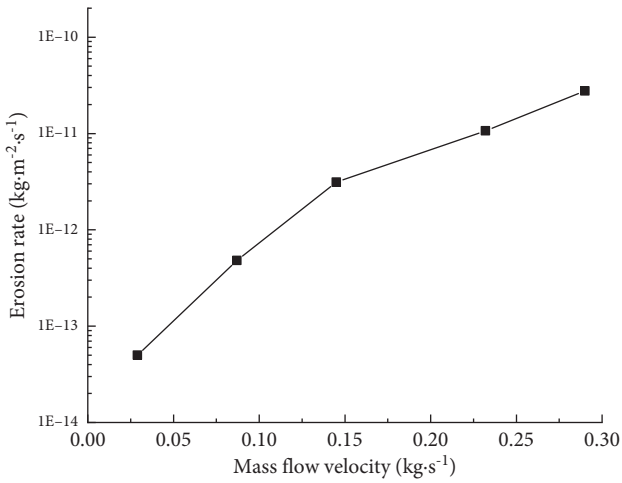

Figure 14: Effect of different mass flow velocities on erosion rates.

increases as the flow velocity increases (see Figure 6), and it leads to an increase in the kinetic energy of the particles carried by the fluid, and the randomness of the particles within the fluid becomes greater, making it easier to impact the wall and cause erosion on the wall surface. It can also be seen that the effect of velocity on the erosion rate is linear.

5. Conclusions

By establishing a triangle subchannel model, the flow heat transfer characteristics of LBE in the core channel and the wall erosion phenomenon by the particulate matter carried in LBE are investigated:

(1) As the inlet velocity increases, the outlet temperature of LBE in the subchannel decreases, the heat transfer coefficient increases, and the overall velocity increases.

(2) The distribution of temperature, velocity, and turbulent energy of LBE in the subchannel is similar, and they all have Y-shaped symmetric distribution.

(3) With the increase of the concentration of particles in the LBE, the erosion rate of particles on the wall increases; when the concentration of particles is less than 1%, the influence of particle concentration on the rate of erosion is small; when the concentration of particles is greater than 1%, the increase in concentration will lead to a sharp increase in the erosion rate of particles on the wall.

(4) As the density of particulate matter within the LBE increases, the erosion rate of particulate matter on the wall gradually decreases. However, the change in density has a low degree of effect on the particulate matter.

(5) As the particle size within the LBE increases, the erosion rate of the particles on the wall becomes larger, and the effect of the change in the particle size of smaller particles is more obvious.

(6) The velocity has the greatest effect on the erosion rate. The greater the velocity, the stronger the erosion capacity of the particles, and the change in the erosion rate is an order of magnitude change.

Data Availability

The data used to support the findings of this study are available from the corresponding author upon request.

Conflicts of Interest

The authors declare that there are no conflicts of interest regarding the publication of this paper.

Acknowledgments

This research was funded by the "13th Five-Year Plan" Project of the Year 2016, under grant number: 2016-JKGHA-0017, and the Open Fund of Key Laboratory of Water-Saving Agriculture of Henan Province, under grant numbers: FIRI2016-19–01 and FIRI2017-20-01."

References

[1] Z. Liu, D. Huang, C. Wang et al., "Flow and heat transfer analysis of lead–bismuth eutectic flowing in a tube under rolling conditions," *Nuclear Engineering and Design*, vol. 382, Article ID 111373, 2021.

[2] T. Abram and S. Ion, "Generation-IV nuclear power: a review of the state of the science," *Energy Policy*, vol. 36, no. 12, pp. 4323–4330, 2008.

[3] Y. Zhang, C. Wang, Z. Lan et al., "Review of thermal-hydraulic issues and studies of lead-based fast reactors," *Renewable and Sustainable Energy Reviews*, vol. 120, Article ID 109625, 2020.

[4] Y. Wang, X. Li, X. Huai, J. Cai, and W. Xi, "Experimental investigation of a LBE-helium heat exchanger based the ADS," *Progress in Nuclear Energy*, vol. 99, pp. 11–18, 2017.

[5] Y. Zhang, C. Wang, R. Cai et al., "Experimental investigation on flow and heat transfer characteristics of lead–bismuth eutectic in circular tubes," *Applied Thermal Engineering*, vol. 180, Article ID 115820, 2020.

[6] X. Cheng and N. I. Tak, "CFD analysis of thermal–hydraulic behavior of heavy liquid metals in sub-channels," *Nuclear Engineering and Design*, vol. 236, no. 18, pp. 1874–1885, 2006.

[7] J. Zhang, "A review of steel corrosion by liquid lead and lead-bismuth," *Corrosion Science*, vol. 51, no. 6, pp. 1207–1227, 2009.

[8] J. J. Park, D. P. Butt, and C. A. Beard, "Review of liquid metal corrosion issues for potential containment materials for liquid lead and lead–bismuth eutectic spallation targets as a neutron source," *Nuclear Engineering & Design*, vol. 196, no. 3, pp. 315–325, 2000.

[9] J. Abella, A. Verdaguer, S. Colominas, K. Ginestar, and L. Martinelli, "Fundamental data: solubility of nickel and oxygen and diffusivity of iron and oxygen in molten LBE," *Journal of Nuclear Materials*, vol. 415, no. 3, pp. 329–337, 2011.

[10] X. Du, S. Liu, P. Liu, X. Yuan, and Y. Zhang, "Numerical simulation of pipeline erosion of particulate matter in LBE based on DPM model," *Nuclear Power Engineering*, vol. 42, no. 01, pp. 48–53, 2021.

[11] L. Liu, T. Zhou, X. Yang, and Z. Su, "Study on performance of pipe in prevention of deposition of particulate matter in liquid LBE," *Huadian Technology*, vol. 36, no. 05, pp. 14–16+22+76, 2014.

[12] J. Chen, T. Zhou, X. Fang, X. Wang, and X. Yang, "Research pf nanoparticles' thermophoresis movement in liquid lead-bismuth eutectic alloy," *Nuclear Science and Engineering*, vol. 037, no. 002, pp. 223–228, 2017.

[13] C. Wang, C. Wang, Y. Zhang et al., "Investigation on flow heat transfer characteristic of lead-bismuth eutectic alloy," *Atomic Energy Science and Technology*, vol. 55, no. 05, pp. 822–828, 2021.

[14] X. Cheng and N.-I. Tak, "Investigation on turbulent heat transfer to lead-bismuth eutectic flows in circular tubes for nuclear applications," *Nuclear Engineering and Design*, vol. 236, no. 4, pp. 385–393, 2006.

[15] J. K. Edwards, B. S. McLaury, and S. A. Shirazi, "Modeling solid particle erosion in elbows and plugged tees," *Journal of Energy Resources Technology*, vol. 123, no. 4, pp. 277–284, 2001.

[16] J. K. Edwards, B. S. McLaury, and S. A. Shirazi, "Evaluation of alternative pipe bend fittings in erosive service," *ASME*, vol. 253, 2000.

[17] I. Finnie, "Erosion of surfaces by solid particles," *Wear*, vol. 3, no. 2, pp. 87–103, 1960.

[18] B. S. McLaury, J. Wang, S. A. Shirazi, J. R. Shadley, and E. F. Rybicki, "Solid particle erosion in long radius elbows and straight pipes," in *Proceedings of the SPE Annual Technical Conference and Exhibition*, OnePetro, San Antonio, TX, USA, October 1997.

[19] G. C. Pereira, F. J. de Souza, and D. A. de Moro Martins, "Numerical prediction of the erosion due to particles in elbows," *Powder Technology*, vol. 261, pp. 105–117, 2014.

[20] M. Parsi, K. Najmi, F. Najafifard, S. Hassani, B. S. McLaury, and S. A. Shirazi, "A comprehensive review of solid particle erosion modeling for oil and gas wells and pipelines applications," *Journal of Natural Gas Science and Engineering*, vol. 21, pp. 850–873, 2014.

[21] D. O. Njobuenwu and M. Fairweather, "Modelling of pipe bend erosion by dilute particle suspensions," *Computers & Chemical Engineering*, vol. 42, pp. 235–247, 2012.

[22] S. He, M. Wang, J. Zhang, W. Tian, S. Qiu, and G. H. Su, "Numerical simulation of three-dimensional flow and heat transfer characteristics of liquid lead-bismuth," *Nuclear Engineering and Technology*, vol. 53, no. 6, pp. 1834–1845, 2021.

[23] K. Mikityuk, "Heat transfer to liquid metal: review of data and correlations for tube bundles," *Nuclear Engineering and Design*, vol. 239, no. 4, pp. 680–687, 2009.

[24] P. A. Ushakov, A. V. Zhukov, and N. M. Matyukhin, "Heat transfer to liquid metals in regular arrays of fuel elements," *High Temperature*, vol. 15, 1978.